Arabian Journal of Geosciences (2020) 13: 292
https://doi.org/10.1007/s12517-020-5280-5

ORIGINAL PAPER

Numerical simulation of the morphological effect of rock joints in the processes of concentrating elastic strain energy: a direct shear study

Xiaojun Feng[1] · Qiming Zhang[1] · Xiaofei Liu[1] · Muhammad Ali[1,2]

Received: 1 June 2019 / Accepted: 3 March 2020 / Published online: 23 March 2020

Abstract

Rockburst in coalmines is the result of the release of the elastic strain energy (ESE) stored in rock and coal masses. The examination of the elastic strain energy (ESE) along rock joint is important to evaluate the shear strength of rock masses. The morphology of joints and the strength of rock masses are considered as the key factors influencing the distribution of the ESE. In this study, a three-dimensional model is developed to quantify the influence of the morphological effect of rock joint (by varying the amplitude and wavelength of the joint) and different materials (coal or rock) on the distribution of the ESE. The results show that when the wavelength of the joint reaches about 5~20% of the length of the model and the amplitude of joint reaches about 2~10% of the height of the model, a relative high concentration of the ESE was found at the left and right crests, together with a low concentration in the middle crests. For most cases, the maximum ESE generally has a similar order of magnitude (10^8~10^9 J) and approximately arched trend for different wave amplitudes for the joints. However, in cases of the flattest joint only reaches about 10^{-16} J. Regarding the influence of different materials on ESE, the rock-rock system generally has a similar distribution of ESE with the rock-coal system, but the latter one concentrates much more ESE. The coal-rock system has the smallest ESE. This recognition of the highly unbalanced distribution of ESE will certainly help to effectively reduce the potential failure of rocks under the CNL boundary conditions.

Keywords Elastic strain energy · Direct shear · Joint morphology · Numerical modeling

Introduction

The evaluation of shear strength of rock-rock and/or rock-coal interfaces is the foundation of geotechnical and mining engineering (Xiong et al. 2019; Yan et al. 2019; Li et al. 2016; Sharma et al. 2018; Jin et al. 2019), such as assessing the stability of the slide of a slope, the design of support and maintenance of roadways in mining or civil engineering, and gravity dams. Normally, the shear strength of the interfaces can be obtained by conducting laboratory direct shear tests or numerical simulations (Brewer and Sleeman 1960; Mackenzie and Garrels 1971; Elliott 1972; Feng et al. 2016a, b, 2018, 2019a, b, c). However, the failure modes of rock-rock and/or rock-coal interfaces are still difficult to accurately clarify and summarize, because they are obviously influenced by the mechanical properties of different materials, morphology of the interfaces, applied shear boundary conditions, and the interaction of different factors (Barton 1973, 1976; Bandis et al. 1983; Grasselli and Egger 2003; Belem et al. 2009; Liu et al. 2018).

A large number of laboratory direct shear tests have been conducted to study the behavior of deformation and evolutionary state of stress under direct shear boundary conditions (Cerato and Lutenegger 2006; Bandis et al. 1981; Dang et al. 2016a, b, 2017a, 2018). By employing different

Responsible Editor: Zeynal Abiddin Erguler

✉ Xiaojun Feng
xiaojun.feng@cumt.edu.cn

✉ Qiming Zhang
QimingZhang@cumt.edu.cn

✉ Xiaofei Liu
liuxiaofei@cumt.edu.cn

✉ Muhammad Ali
muhammad.ali@cumt.edu.cn

[1] School of Safety Engineering, China University of Mining and Technology, Xuzhou 221116, China

[2] Department of Mining Engineering, Balochistan University of Information Technology, Engineering and Management Sciences, Quetta, Pakistan

boundary conditions, the studies of joint shear behavior were mainly contributed by Dang et al. (2016a, b, 2017a, 2018)) by using GS-1000 big shear box device, including the direct and cyclic shear behaviors under CNL boundary conditions, the direct and cyclic shear behavior of jointed rock under DNL conditions. Their works provide direct evidence to help deeply understand the affecting parameters of the normal stress level, direct shear rate, horizontal cyclic shear frequency and normal impact frequency, horizontal cyclic shear displacement amplitude, and vertical impact force amplitude in the shear behaviors (Dang 2016). Currently, compared to the traditional mold customization methods for conducting laboratory tests, the 3D printing technology in geotechnical engineering (Ishutov et al. 2015; Jiang et al. 2016; Fereshtenejad and Song 2016) became widespread due to the lower cost and more infinitely malleable features when designing the shape of model. For instance, on the basis of using the 3D printing technology, Liu et al. (2018) has presented the joint description by involving the apparent dip angle and joint height. They demonstrated that the surface morphology and normal stress have a significant influence in the peak stress strength and the distribution of the damage area. But the consistence between the strength of printed materials and natural rocks needs further studies (Fereshtenejad and Song 2016).

The shearing behaviors of rock joint under direct shear boundary conditions were widely discussed (Goodman and Brown 1962; Park and Song 2009; Zhang and Thornton 2007; Lobo-Guerrero and Vallejo 2005; Liu et al. 2005; Karami and Stead 2008; Yan 2009; Son et al. 2004; Oh et al. 2017; Dang et al. 2019a, b), Park and Song (2009) used contact bond model (PFC code) to reproduce a rock joint. They demonstrated that the coefficient of friction of modeling material acts as the most important parameter controlling the strength of shear and dilation angle. In addition, the cohesion is influenced much more than the peak friction when varying the roughness of reproduced joint and the strength of contact bond in the model. Oh et al. (2017) quantified the effects of normal stresses and wavelength values of joints on the dilation behavior. Their results also show that the magnitude of normal stress is more important as compared to other parameters. Dang et al. (2017b) duplicated the lab direct shear test completely using FLAC 3D to simulate the test device including the specimen. With the duplicated device, they observed the rotation of the upper blocks of specimen and the inhomogeneous distribution of stress along the joint during direct shear tests. However, the distribution of the ESE resulted from inhomogeneous stress along the joints under CNL boundary conditions remains unexplored in previous works, which might be important for geotechnical and mining engineering.

The ESE along the interface is a key factor in understanding the process of strain/deformation concentration and the release under CNL boundary conditions. Exploring the distribution and evolution of the ESE could also help to locate the areas with high energy, and subsequently take certain (e.g., weakening the materials) actions to release energy. A series of laboratory and numerical tests have been conducted to explore the relationship among shearing strength, the morphology of interface, and the strength of materials and external boundary conditions. However, the fact remains that it would be more interesting to quantify the influence of the morphology of interface phenomenon (by varying the amplitude and wavelength of the interface) and the strength of materials on the distribution of the ESE, as it is important to design the support of rock masses with pre-existing joints and to accurately release the concentration of the ESE in geotechnical and mining engineering.

Numerical method and model setup

The evaluation of shear strength of rock-rock and/or rock-coal interfaces is the foundation of geotechnical engineering and mining. This three-dimensional model was established using the structural mechanics module of COMSOL Multiphysics software. The geometry of the model is shown in Fig. 1. The designed model domain is 300 mm long in X direction, 180 mm wide in Z direction, and 150 mm high in Y direction. It is composed of an upper block and a lower block; the interface between these two blocks is subject to a waveform with different amplitudes and wavelengths. In order to mainly focus on exploring the shear behavior of the interface morphology between the upper and lower blocks, the following assumptions are considered in the model: (1) The coal and rock masses are treated as elastic medium, and the relationship between stress and strain of the coal and rock masses is subject to Hooke's law; (2) coal and rock masses are homogeneous medium, that is, all coal and rock formations are composed of the same material; (3) the coal and rock bodies are isotropic medium, that is, the physical properties of the objects are same in all directions. The equation of motion (Eq. 1) in the modeling code is expressed as follows:

$$\rho \frac{\partial^2 u}{\partial t^2} = \nabla \cdot P + Fs \tag{1}$$

where ρ is the density corresponding to the materials density in the initial undeformed state, Fs is the volume force vector, and P is the first Piola-Kirchhoff stress.

The displacement component and strain component of the three directions satisfy the geometric Eq. (2), which is expressed as tensor symbol:

$$\varepsilon_{ij} = \frac{1}{2}\left(u_{i,j} + u_{j,i}\right) \tag{2}$$

where ε_{ij} is the strain component ($i, j = 1, 2, 3$); u_i is the displacement component in the direction.

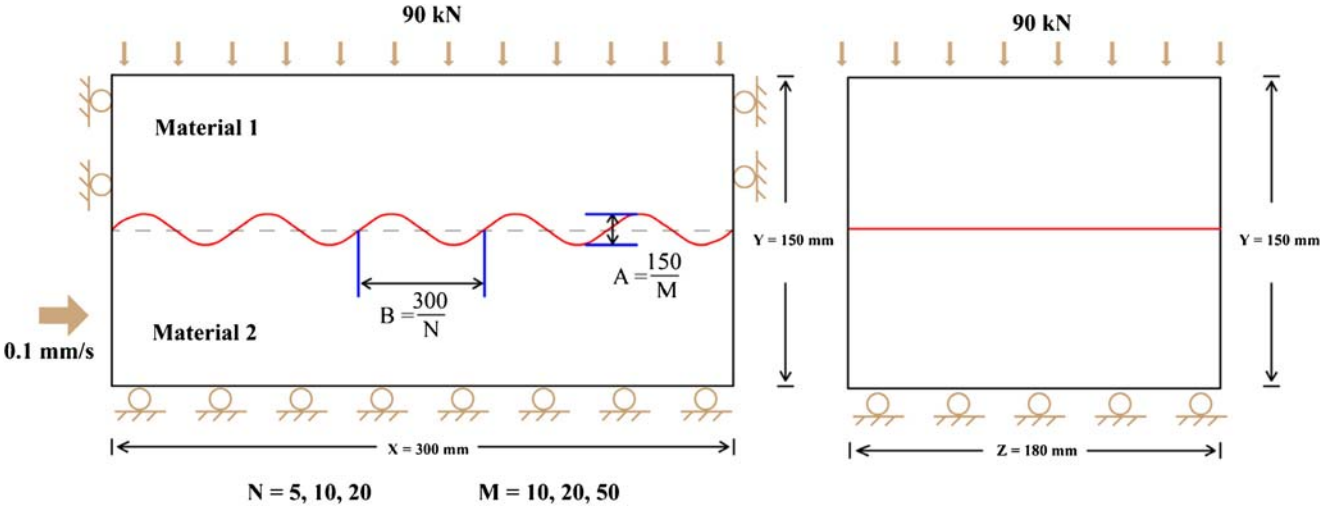

Fig. 1 Model geometry and the used CNL boundary conditions. Materials 1 and 2 represent different materials (rock or coal masses). The red line in the model presents the joint. The parameters for characterizing the joint morphology between the upper and lower blocks are presented in Table 1

The constitutive equation is the equation to characterize the relationship between medium stress and strain of coal and rock masses. According to the above basic assumption, the deformation of coal and rock is linear elasticity, and the constitutive relationship between stress and strain conforms to the generalized Hooke's law:

$$\delta_{ij} = \lambda\varepsilon_V + 2G\varepsilon_{ij} \tag{3}$$

where λ is the Lame constant, $\lambda = 2Gv/(1-2v)$; ε_V is the volume strain, $\varepsilon_V = \varepsilon_{11} + \varepsilon_{22} + \varepsilon_{33}$; G is the shear modulus, $G = E/2(1+v)$.

In order to comprehensively analyze the influence of the morphology of rock-rock and rock-coal interfaces on the ESE in geotechnical and mining engineering, the common morphology of the joints in nature was selected, fitted, and standardized. The parameters of coal and rock are determined as shown in Table 1. The strain energy density function has the following expression: $W_s = \frac{1}{2}(\sigma_i + \sigma)\varepsilon_{e1}$, where σ_i is the initial stress. In this numerical simulation, we applied a normal stress of 90 kN on the top of the model to simulate the self-weight of the coal/rock beds and the stress generated by the structure, and the bottom was fixed. On both sides of the model, the upper block was constrained in horizontal direction. A constant velocity of 0.1 mm/s was applied on the left side of the lower block of the model. This boundary condition is shown in Fig. 1. The other parameters for characterizing the morphology of the joint between the upper and lower blocks are presented in Table 2.

Table 1 Mechanical parameters of different materials

Parameter		Symbol	Value-units
Rock (granite)	Density	ρ_r	2700 kg/m^3
	Young's modulus	E_r	5×10^{10} Pa
	Poisson's ratio	v_r	0.27
Coal	Density	ρ_c	1500 kg/m^3
	Young's modulus	E_c	2×10^{9} Pa
	Poisson's ratio	v_c	0.3
Amplitude of waveform		A	–
Wavelength of waveform		B	–
Gravitational acceleration		g	9.81 m/s^2

Results

ESE influenced by joint morphology

B was set to 15 mm

When the joint between the upper and lower block yields a relative compact (high frequency character) wavelength (15 mm), the ESE generally shows a similar distribution when using the different amplitudes (3~15 mm) for the model, reaching an order of magnitude 10^8 J for all red points on the chosen crests (Fig. 2). The stored ESE at crests is commonly greater than that around the troughs and the middle points between crests and troughs. Regarding the ESE stored at different crests, the right-most crest always concentrates the largest ESE compared to other three crests in these three cases (Fig. 2). For the two crests located in the middle areas of the interface, the ESE concentrated at them reaches up to about 25~40% of the ESE stored on their left and right sides for cases rr1 and rr3. For the interface having a moderate amplitude (case rr2), the ESE in the middle crests is only up to about 13~43% of that in their left and right crests, showing a relatively

Table 2 Experiments name and related parameters for characterizing the joint in the model

Exp#	Material 1	Material 2	A (mm)	B (mm)
rr1	Rock	Rock	15	15
rr2	Rock	Rock	7.5	15
rr3	Rock	Rock	3	15
rr4	Rock	Rock	15	30
rr5	Rock	Rock	7.5	30
rr6	Rock	Rock	3	30
rr7	Rock	Rock	15	60
rr8	Rock	Rock	7.5	60
rr9	Rock	Rock	3	60
cr1	*Coal*	Rock	15	15
rc1	Rock	*Coal*	15	15
cr2	*Coal*	Rock	15	30
rc2	Rock	*Coal*	15	30
cr3	*Coal*	Rock	7.5	15
rc3	Rock	*Coal*	7.5	15
cr4	*Coal*	Rock	7.5	30
rc4	Rock	*Coal*	7.5	30

high uneven distribution compared to other two cases. Overall, high concentration of the ESE is all stored in the crests (red points in Fig. 2) compared to other positions (black points in Fig. 2) used to record the ESE in the rock-rock system under the CNL boundary conditions. This suggests that, from the perspective of ignoring the size effect under the CNL boundary conditions, when the wavelength of the interface reaches about 5% of the length of the model and the amplitude of interface reaches about 2~10% of the height of the model, a certain characteristic in the distribution of the ESE can be concluded, thus resulting in a relative high concentration of the ESE in the left and right crests and low concentration in the middle crests. Regarding some high-ESE black points on the left-most part of the model, increase in the concentration of the ESE over the process of direct shearing is certainly due to the velocity directly applied on the left side of the lower block. In the view of ignoring the length effect, the ESE recorded in the middle part can definitely help to understand the distribution of the ESE at the interface.

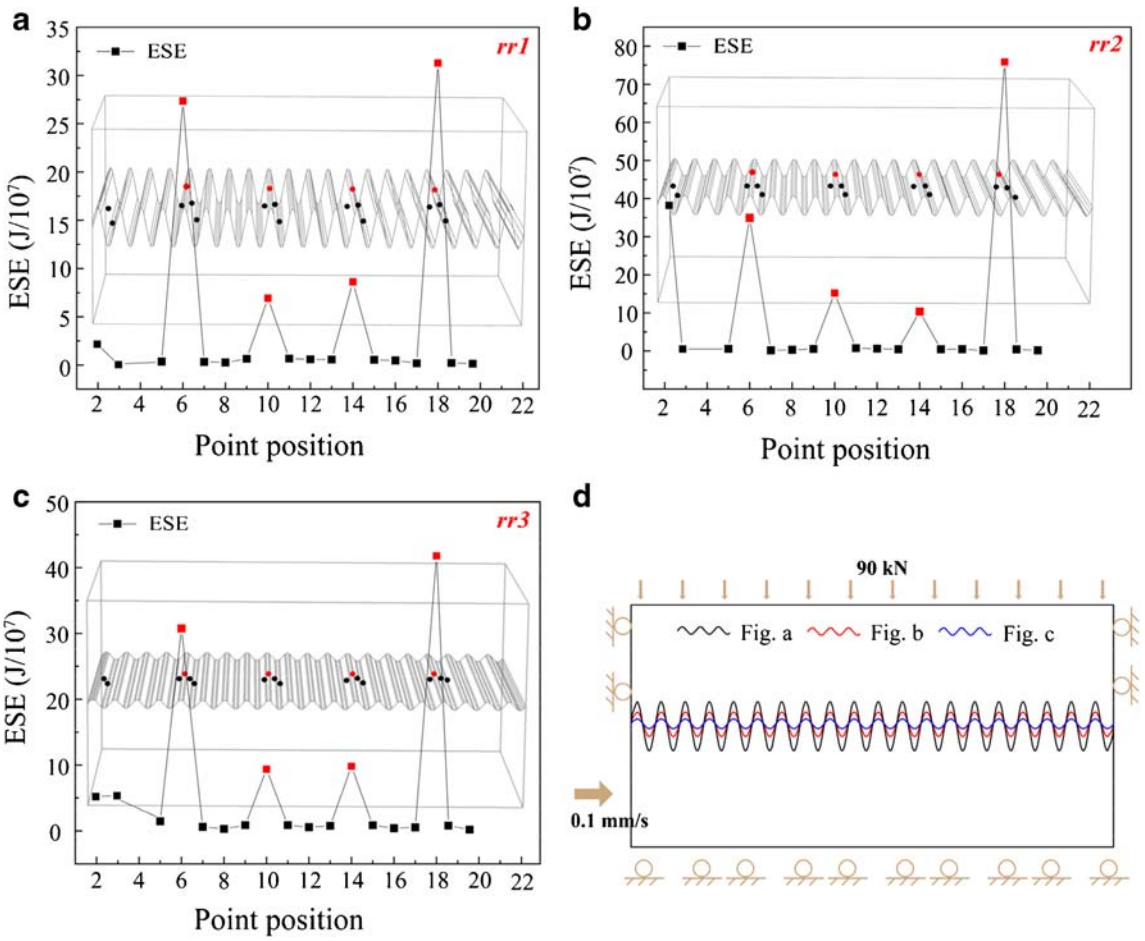

Fig. 2 The distribution of the ESE influenced by the different amplitudes of the interface between these two blocks when the wavelength was set to 15 mm

B was set to 30 mm

With the increase of the wavelength characterizing the interface between the blocks ($B = 30$ mm, Fig. 3), the maximum ESE stored in the right crest for cases rr4 and rr4 increases an order of magnitude compared to other cases with B equaling to 15 mm, which reaches at about 10^9 J. For the case rr4, it shows a similar distribution and magnitude of the ESE with the previous mentioned cases rr1~rr3 in "B was set to 15 mm" section, showing the low ESE in the middle and the highest ESE in the left sides of the model, respectively. For cases rr5 and rr6, the ESE stored in the right-most crest designed in the interface greatly increases compared to that in case rr4, reaching about 19.5~50.2 times than the ESE concentrated in other crests (red points in Fig. 3). This indicates that when the wavelength of the interface reaches about 10% of the length of the model and the amplitude of interface reaches about 2~5% of the height of the model, a significant concentration of the ESE could be located on the interface where is the right part of the model. Using this info, certain actions for releasing the ESE would be effectively invalided in protecting against rockburst, slope sliding, etc., under the CNL boundary conditions.

B was set to 60 mm

When the wavelength was lengthened to 60 mm, it means that there are six full cycles for composing of the interface between the two blocks (Fig. 4). Overall, the ESE decreases with the decreasing amplitude characterizing the interface (follow the order, rr7, rr8, and rr9 in Fig. 4). For cases rr7 and rr8, the maximum ESE (about 10^9 J) was observed at the rightmost crests. This feature is similar with the cases in Figs. 2 and 3. Regarding the of the ESE at different crests of the interface, also showing that the ESE observed at the middle crests is relatively lower than that at the left and right crests (only reach about 4.9~6.7% for case rr7 and 9.5~13.1% for case rr8 of the ESE at the rightmost crests). This highly imbalanced distribution of the ESE indicates that locating the location of the maximum ESE could definitely help effectively reduce the potential failure of rocks when rock or coal masses consist of pre-existing interfaces in engineering. With respect to case rr9 (the amplitude reduces to 3 mm), the ESE becomes significantly low no matter where it is stored at the interface, only up to about 10^{-16} J, and the distribution for the ESE at the designed

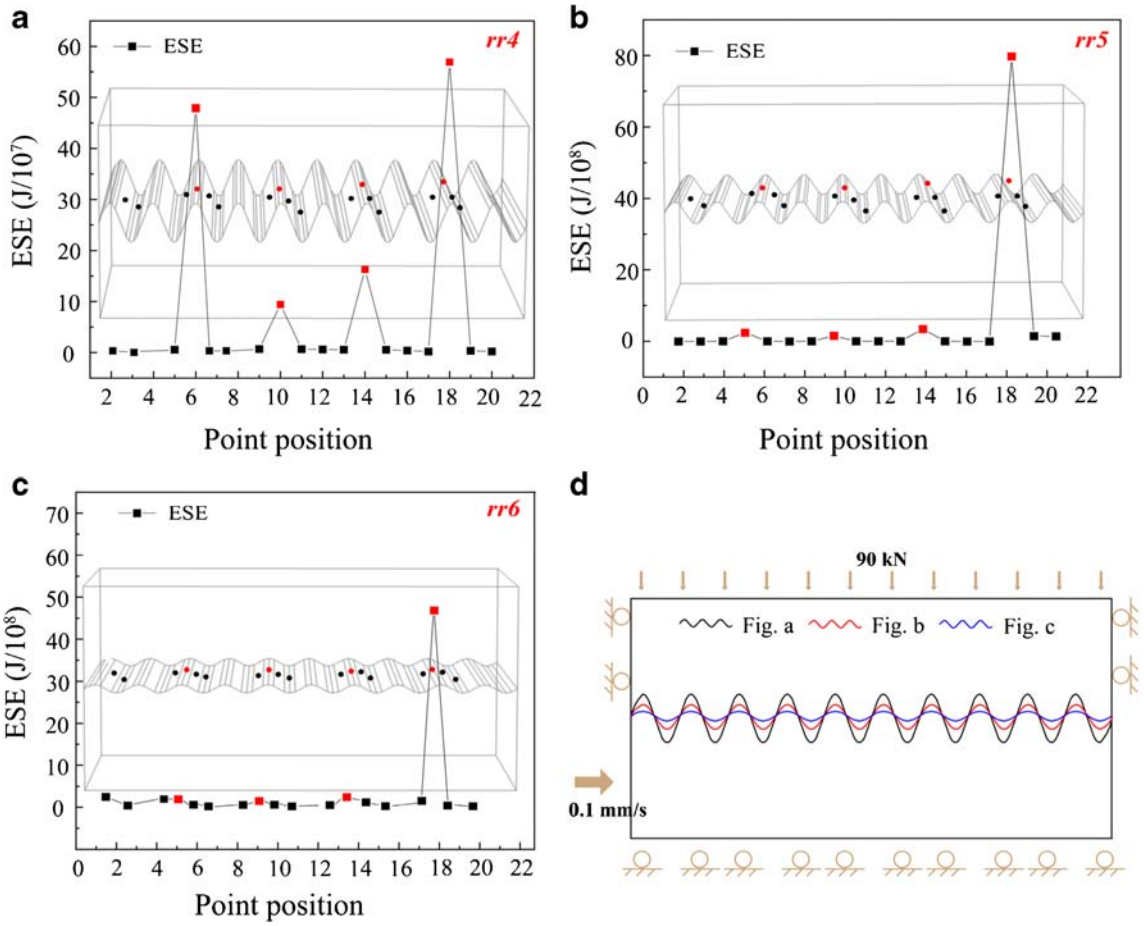

Fig. 3 The distribution of ESE influenced by the different amplitudes of the interface between these two blocks when the wavelength was set to 30 mm

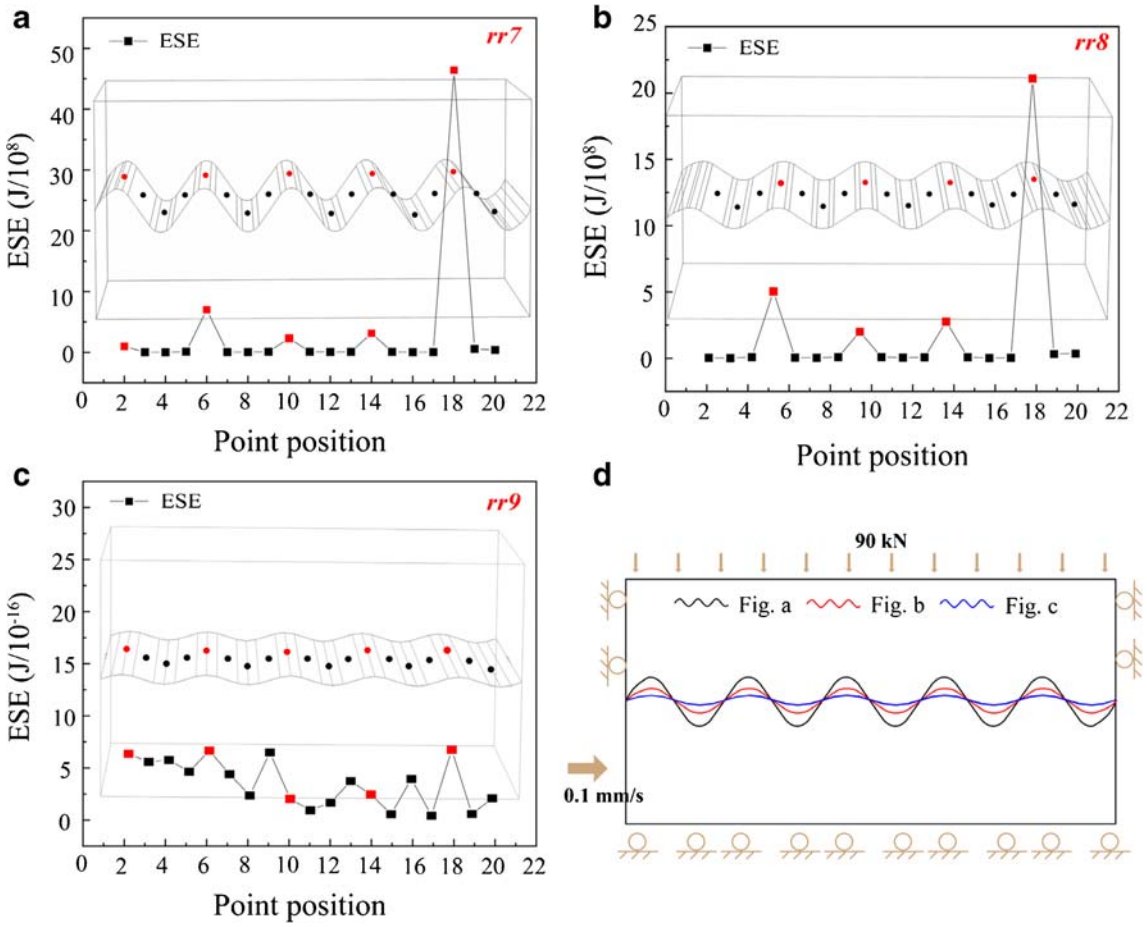

Fig. 4 The distribution of ESE influenced by the different amplitudes of the interface between these two blocks when the wavelength was set to 60 mm

locations (red and black points) is quite fluctuated. Although this fluctuated ESE has a low value, the difficulty in recognizing the maximum ESE is high. With the increase of loading time on the model, the ESE will significantly increase, but locating the maximum ESE in the system would still be difficult. This indicates that although a relatively low ESE produced when employing the flattest interface (when B was set to 60 mm), the uncertainty in finding the mostly potential failure in rock or coal masses when consisting of pre-existing interfaces would increase.

Maximum and mean ESE

The ESE stored in rock and/or coal is widely accepted as a key factor inducing rockburst in mining engineering (Kidybiński 1981; Linkov 1996; Wang and Park 2001; Ansell 2005; Wang et al. 2006), as it could release suddenly at a high rate when the deformation of rocks exceeds the limitation (Tang and Kaiser 1998; Zhu et al. 2010). The distribution of the ESE at crests in the model has been examined in Figs. 2, 3, and 4. In order to compare the maximum and mean ESE in the model when the interface between the upper and lower blocks employs different wavelengths and amplitudes, for rock-rock system, the ESE in different cases is presented in Fig. 5.

In Fig. 5, the results show that the maximum ESE (red line in Fig. 5) generally has a similar order of magnitude (10^8~10^9) and an approximately arched trend when designing different wave amplitudes for the interface (from case rr1~case rr8). Particularly, case rr9 (Fig. 4c, d) has the flattest interface compared to other cases; it is only up to an order of magnitude 10^{-16} for the maximum ESE suggesting that under the CNL boundary conditions, a relatively high amplitude employed for the interface favors high concentration of the ESE. Regarding the mean ESE concentrated in different cases, it generally yields a range order of magnitude (10^7~10^8) for cases rr1~case rr8. For the mean ESE influenced by different amplitudes characterizing the interface, it shows an arched trending which is similar with the maximum ESE. It also suggests that a moderate amplitude of the joints favors concentrating the largest mean ESE (cases rr2 and rr5).

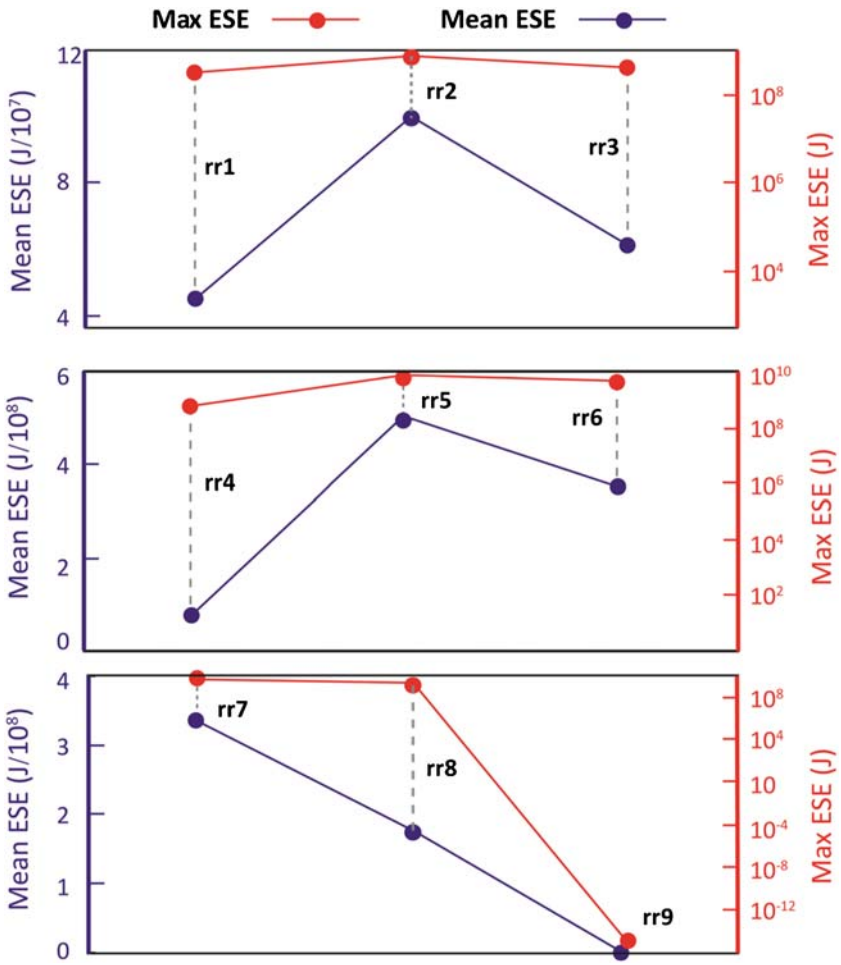

Fig. 5 Maximum and mean ESE for all chose points in the model as indicated in Figs. 2, 3, and 4. Red line represents the mean ESE of all points for different models in Table 2. Dark blue shows the maximum ESE of all plotted points in the model

Discussion

Effect of rock strength

Inherited structures or interfaces such as fault zones or joints exist in almost any rock or/and coal masses. In most situations, these inherited structures have an important role in the failure behavior and mechanism of rock or coal masses (Lambert and Coll 2014) when re-activation (Walsh et al. 2002; Bellahsen and Daniel 2005) takes place due to the broken energy balance in the system (Hu et al. 2019; Feng et al. 2019d). The morphology of interface and the strength of rocks are two key impactors controlling the deformation and strength of the rock or/and coal masses (Borri-Brunetto et al. 1999; Strom 2006; Ghazvinian et al. 2010; Feng et al. 2018). Regarding the ESE under the CNL boundary conditions (Fardin et al. 2004), the anisotropy and the interface morphology of materials are thought to play a key role in influencing the distribution of the ESE when the external boundary conditions applied changes (stress and/or velocity fields). Regarding the direct shear tests under the CNL boundary condition, the mechanical properties of the upper and lower blocks and the amplitude and wavelength of the interface between them characterizing their morphology were both examined in detailed in this study. The results show that the rock-rock system (cases rr1 and rr4) has a similar distribution of the ESE with the rock-coal system (cases rc1 and rc2) generally, but the latter one concentrates much more ESE (with a maximum ESE of 4.2×10^8 J in case rc1 and 1.37×10^9 J in case rc2 stored at the left-side crest as shown in Fig. 6). This is probably due to the fact that a relatively softer lower block tends to generate more deformation under the CNL boundary condition as compared to the model consisting of a hard lower-block. In particular, the coal-rock system (cases cr1 and cr2 in Fig. 6) has the smallest ESE compared to the others. Additional ESE recorded at crests of the interface presents a high volatility and inconsistence compared to the other cases (e.g., cases rr1 and rc1; rr4 and rc2). The reason is that a soft upper-block plays the role of a relatively weak medium in transferring stress that results in a low concentration of the ESE in the system under the CNL boundary conditions. Indeed, the roughness of interface represents a

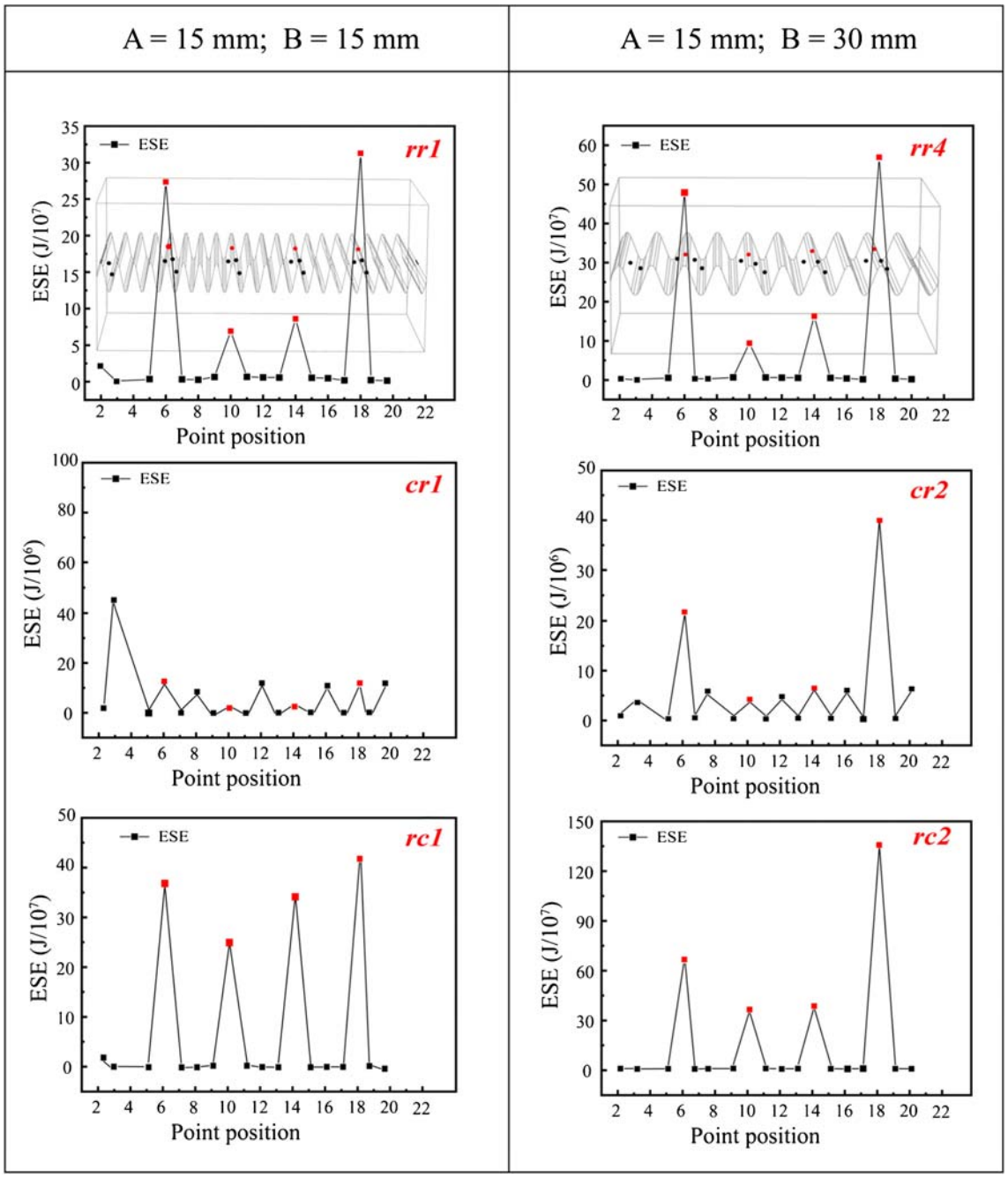

Fig. 6 The distribution of the ESE at the interface when the upper and lower blocks of the model were modeled with different materials (coal or rock masses). The model in the first column has parameters $A = 15$ mm and $B = 15$ mm for characterizing the joint morphology, while it has parameters of $A = 15$ mm and $B = 30$ mm in the second column

prefect waveform, but these preliminary tests can also help understand the distribution of deformation and ESE influenced by the amplitudes and wavelength of the interface under the CNL boundary conditions. The limitations in pre-producing the roughness of the interface can be effectively improved when a 3D laser scanner (Fardin et al. 2004; Sturzenegger and Stead 2009) can be used in situ, by incorporating scanned interface roughness data into the modeling domain.

Timing effect of concentrating ESE

The ESE is commonly influenced by the duration of constant or dynamic loading applied on the model, the strength of rock masses, and the damage-induced anisotropy of the model (Emery 1964; Friedman 1972; Sih 1974; Bieniawski 1967). The evolution of the ESE in case rr4 was examined in Fig. 7. The ESE information carried by four red points located at crests of the interface between the upper and lower blocks in

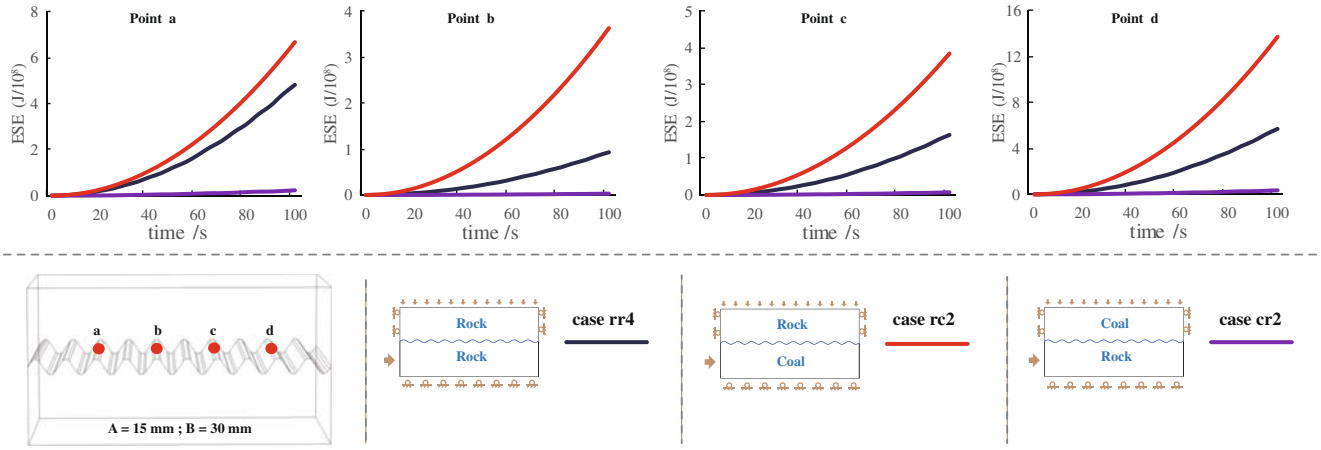

Fig. 7 The effect of time on the accumulation of the ESE influenced by different materials assigned to the two blocks. Four red points are located at crests in the model. Dark blue = rock-rock system; red line = rock-coal system; purple line = coal-rock system

the model was tracked. In general, the ESE increases with the duration of the constant normal loading and velocity applied on the model. The results show that the ESE concentrated at crests a and d presents a faster rate and greater amount compared to that at crests b and c.

In civil and mining engineering, such as tunnel excavation in rock and/or coal masses, rockburst normally occurs at a relatively high frequency in surrounding rock or coal, which results from the highly concentrated ESE in the materials. With the increase in the anisotropy of materials (Hoek and Brown 1980; Wang et al. 2009; Su et al. 1998; Hoek 1964; Schormair et al. 2006), the distribution of stress and strain will show a high irregular character when conducting tunnel excavation. This certainly increases the complexity in reducing rockburst disaster. The interface morphology is key parameter to characterize the contacting relationship of different materials. In order to explore the ESE influenced by different materials assigned to the upper and lower blocks (rock or coal), thus rock-rock, rock-coal and coal-rock systems were constructed (Table 2, Fig. 7).

Figure 7 shows that the rock-coal system concentrates the largest ESE compared to rock-rock and coal-rock systems. At points a and b, rock-rock and rock-coal systems show the maximum (71.5% of rock-coal system) and minimum (26% of rock-coal system) ESE respectively compared to that obtained at points c and d. At points c and d, the ESE in the rock-rock system reaches about 41.5–42.3% of that obtained in the rock-coal system. This significant difference in the distribution and evolution of the ESE is probably due to the excessive difference in material strength between coal and rock masses (Feng and Zhang 2018). When the lower block is compressed, a relative displacement will occur between the upper and the lower blocks with the structural bodies resisting deformation and generating ESE in the interior. As time goes on, the ESE increases gradually with the increase in the relative difference in displacement, and the trending of growth presents an exponential change (Song 2012; Yao et al. 2009). At this point, if the strength of material is the same (rock-rock system), then the ESE dissipates partially to offset the deformation, making the energy accumulation rate slow. When the strength of the upper material is large (rock-coal system), the deformation of the material is small and the ESE cannot be dissipated, resulting in a large energy accumulation. If the strength of the upper material is small (coal-rock system), the deformation of the material will be large, the energy will be released in the deformation process, and only a small amount of ESE will remain. The more different the materials are, the more obvious this rule is.

Conclusions

In this study, a three-dimensional model is developed to quantify the influence of the morphological effect of a rock joint (by varying the amplitude and wavelength of the joint) and different materials (coal or rock masses) on the distribution of the ESE.

1. A relative high concentration of the ESE in the left and right crests and a low concentration in the middle crests were observed, when the wavelength of the joint reaches about 5~20% of the length of the model and the amplitude of joint reaches about 2~10% of the height of the model.
2. The maximum ESE generally has a similar order of magnitude (10^8~10^9) when designing different wave amplitudes for the joint. Whereas for the case having the flattest joint only reaches about 10^{-16}, but the distribution for the ESE is quite fluctuated and therefore the difficulty in recognizing the maximum ESE is high. It also suggests that a moderate amplitude of the joints favors concentrating the largest mean ESE
3. Regarding the ESE influence by different materials, the rock-rock system has a similar distribution of the ESE with the rock-coal system generally, but the latter one concentrates much more ESE. The coal-rock system has the smallest ESE.

Acknowledgments The editors and two anonymous reviewers are warmly thanked for providing very constructive comments.

Funding information This research was funded by the Priority Academic Program Development of Jiangsu Higher Education Institutions (PAPD), and the National Science Foundation for Young Scientists of Jiangsu Province (BK20180644), the Fundamental Research Funds for the Central Universities (2018QNB01), and China Postdoctoral Science Foundation (2019M652021).

References

Ansell A (2005) Laboratory testing of a new type of energy absorbing rock bolt. Tunn Undergr Space Technol 20(4):291–300. https://doi.org/10.1016/j.tust.2004.12.001

Bandis S, Lumsden AC, Barton NR (1981) Experimental studies of scale effects on the shear behaviour of rock joints. Int J Rock Mech Min Sci Geomech Abstr 18(1):1–21. https://doi.org/10.1016/0148-9062(81)90262-X

Bandis S, Lumsden AC, Barton NR (1983) Fundamentals of rock joint deformation. Int J Rock Mech Min Sci Geomech Abstr 20(6):249–268. https://doi.org/10.1016/0148-9062(83)90595-8

Barton N (1973) Review of a new shear-strength criterion for rock joints. Eng Geol 7:287–332. https://doi.org/10.1016/0013-7952(73)90013-6

Barton N (1976) The shear strength of rock and rock joints. Int J Rock Mech Min Sci Geom Abstr 13:255–279. https://doi.org/10.1016/0148-9062(76)90003-6

Belem T, Souley M, Homand F (2009) Method for quantification of wear of sheared joint walls based on surface morphology. Rock Mech Rock Eng 42(6):883–910 http://sci-hub.tw/10.1007/s00603-008-0023-z

Bellahsen N, Daniel JM (2005) Fault reactivation control on normal fault growth: an experimental study. J Struct Geol 27(4):769–780. https://doi.org/10.1016/j.jsg.2004.12.003

Bieniawski ZT (1967) Mechanism of brittle fracture of rock: part I—theory of the fracture process. Int J Rock Mech Min Sci Geomech Abstr 4(4):395–406. https://doi.org/10.1016/0148-9062(67)90030-7

Borri-Brunetto M, Alberto C, and Bernardino C (1999) Scaling phenomena due to fractal contact in concrete and rock fractures. Fracture Scaling. Springer, Dordrecht, 221-238. http://sci-hub.tw/10.1007/978-94-011-4659-3_12, 1999

Brewer R, Sleeman JR (1960) Soil structure and fabric: their definition and description. J Soil Sci 11(1):172–185. https://doi.org/10.1111/j.1365-2389.1960.tb02213.x

Cerato AB, Lutenegger AJ (2006) Specimen size and scale effects of direct shear box tests of sands. Geotech Test J 29(6):507–516. https://doi.org/10.1520/GTJ100312

Dang W (2016) Shear behavior of plane joints under CNL and DNL conditions: lab testing and numerical simulation, Technischen Universität Bergakademie Freiberg, theses

Dang W, Konietzky H, Frühwirt T (2016a) Rotation and stress changes of a plane joint during direct shear tests. Int J Rock Mech Min Sci 89:129–135. https://doi.org/10.1016/j.ijrmms.2016.09.004

Dang W, Konietzky H, Frühwirt T (2016b) Direct shear behaviour of a plane joint under dynamic normal load (DNL). Eng Geol 213:133–141. https://doi.org/10.1016/j.enggeo.2016.08.016

Dang W, Konietzky H, Frühwirt T (2017a) Direct shear behavior of planar joints under cyclic normal load conditions: effect of different cyclic normal force amplitudes. Rock Mech Rock Eng 50(4):1–7

Dang W, Konietzky H, Herbst M, Frühwirt T (2017b) Complex analysis of shear box tests with explicit consideration of interaction between test device and sample. Measurement 102:1–9. https://doi.org/10.1016/j.measurement.2017.01.040

Dang W, Konietzky H, Chang L, Frühwirt T (2018) Velocity-frequency-amplitude-dependent frictional resistance of planar joints under dynamic normal load (DNL) conditions. Tunn Undergr Space Technol 79:27–34. https://doi.org/10.1016/j.tust.2018.04.038

Dang W, Konietzky H, Frühwirt T, Herbst M (2019a) Cyclic frictional responses of planar joints under cyclic normal load conditions: laboratory tests and numerical simulations. Rock Mech Rock Eng 53:337–364. https://doi.org/10.1007/s00603-019-01910-9

Dang W, Wu W, Konietzky H, Qian J (2019b) Effect of shear-induced aperture evolution on fluid flow in rock fractures. Comput Geotech 114:103152

Elliott D (1972) Deformation paths in structural geology. Geol Soc Am Bull 83(9):2621–2638. https://doi.org/10.1130/0016-7606(1972)83[2621:DPISG]2.0.CO;2

Emery CL (1964) Strain energy in rocks. In: State of Stress in the Earth's Crust, pp 234–279

Fardin N, Feng Q, Stephansson O (2004) Application of a new in situ 3D laser scanner to study the scale effect on the rock joint surface roughness. Int J Rock Mech Min Sci 2(41):329–335. https://doi.org/10.1016/S1365-1609(03)00111-4

Feng X, Zhang Q (2018) The effect of backfilling materials on the deformation of coal and rock strata containing multiple goaf: a numerical study. Minerals 8:224. https://doi.org/10.3390/min8060224

Feng X, Amponsah PO, Martin R, Ganne J, Jessell MW (2016a) 3-D numerical modelling of the influence of pre-existing faults and boundary conditions on the distribution of deformation: example of North-Western Ghana. Precambrian Res 274:161–179. https://doi.org/10.1016/j.precamres.2015.06.006

Feng X, Jessell MW, Amponsah PO, Martin R, Ganne J, Liu D, Batt G (2016b) Effect of strain-weakening on Oligocene-Miocene self-organization of the Australian - Pacific plate boundary fault in southern New Zealand: insight from numerical modelling. J Geodyn 100:130–143. https://doi.org/10.1016/j.jog.2016.03.002

Feng X, Wang E, Ganne J, Amponsah P, Martin R (2018) Role of volcano-sedimentary basins in the formation of greenstone-Granitoid belts in the west African Craton: a numerical model. Minerals 8(2):73. https://doi.org/10.3390/min8020073

Feng X, Zhang Q, Ali M (2019a) Explosion-induced stress waves propagation in interacting faults system: numerical modelling and implications for Chaoyang Coal Mine. Shock Vib. https://doi.org/10.1155/2019/5856080

Feng X, Wang E, Amponsah PO, Ganne J, Martin R, Jessell MW (2019b) Effect of pre-existing faults on the distribution of lower crust exhumation under extension: numerical modelling and implications for NW Ghana. Geosci J 23(6):961–975

Feng X, Wang E, Ganne J, Martin R, Jessell M (2019c) The exhumation along the Kenyase and Ketesso shear zones in the Sefwi terrane, West African Craton: a numerical study. Geosci J 23(3):391–408

Feng X, Zhang Q, Ali M (2019d) 3D modelling of the strength effect of backfill-rocks on controlling rockburst risk: a case study. Arab J Geosci 13(3):128

Fereshtenejad S, Song JJ (2016) Fundamental study on applicability of powder-based 3D printer for physical modeling in rock mechanics. Rock Mech Ock Eng 49(6):2065–2074 http://sci-hub.tw/10.1007/s00603-015-0904-x

Friedman M (1972) Residual elastic strain in rocks. Tectonophysics 15(4):297–330. https://doi.org/10.1016/0040-1951(72)90093-5

Ghazvinian AH, Taghichian A, Hashemi M, Mar'Ashi S (2010) The shear behavior of bedding planes of weakness between two different rock types with high strength difference. Rock Mech Rock Eng 43(1):69–87 http://sci-hub.tw/10.1007/s00603-009-0030-8

Goodman LE, Brown CB (1962) Energy dissipation in contact friction: constant normal and cyclic tangential loading. J Appl Mech 29(1):17–22. https://doi.org/10.1115/1.3636453

Grasselli G, Egger P (2003) Constitutive law for the shear strength of rock joints based on three-dimensional surface parameters. Int J Rock Mech Min Sci 40:25–40. https://doi.org/10.1016/S1365-1609(02)00101-6

Hoek E (1964) Fracture of anisotropic rock. J S Afr Inst Min Metall 64(10):501–523

Hoek E, Brown ET (1980) Empirical strength criterion for rock masses. J Geotech Geoenviron Eng 106(ASCE 15715). http://worldcat.org/oclc/3519342

Hu S, Pang S, Yan Z (2019) A new dynamic fracturing method: deflagration fracturing technology with carbon dioxide. Int J Fract 220:99–111. https://doi.org/10.1007/s10704-019-00403-8

Ishutov S, Hasiuk FJ, Harding C, Gray JN (2015) 3D printing sandstone porosity models. Interpretation 3(3):49–61. https://doi.org/10.1190/INT-2014-0266.1

Jiang Q, Feng X, Gong Y, Song L, Ran S, Cui J (2016) Reverse modelling of natural rock joints using 3D scanning and 3D printing. Comput Geotech 73:210–220. https://doi.org/10.1016/j.compgeo.2015.11.020

Jin A, Wang B, Zhao Y, Wang H, Feng H, Sun H, Yang Z (2019) Analysis of the deformation and fracture of underground mine roadway by joint rock mass numerical model. Arab J Geosci 12(18):559

Karami A, Stead D (2008) Asperity degradation and damage in the direct shear test: a hybrid FEM/DEM approach. Rock Mech Rock Eng 41(2):229–266 http://sci-hub.tw/10.1007/s00603-007-0139-6

Kidybiński A (1981) Bursting liability indices of coal. Int J Rock Mech Min Sci Geomech Abstr 18(4):295–304. https://doi.org/10.1016/0148-9062(81)91194-3

Lambert C, Coll C (2014) Discrete modeling of rock joints with a smooth-joint contact model. J Rock Mech Geotech Eng 6(1):1–12. https://doi.org/10.1016/j.jrmge.2013.12.003

Li H, Liu Y, Li J, Yang F, Liu T, Xia X, Liu B (2016) Numerical study on oblique incidence across rock masses with linear and nonlinear joints. Arab J Geosci 9(1):20

Linkov AM (1996) Rockbursts and the instability of rock masses. Int J Rock Mech Min Sci Geomech Abstr 33(7):727–732. https://doi.org/10.1016/0148-9062(96)00021-6

Liu SH, Sun DA, Matsuoka H (2005) On the interface friction in direct shear test. Comput Geotech 32(5):317–325. https://doi.org/10.1016/j.compgeo.2005.05.002

Liu Q, Tian Y, Ji P, Ma H (2018) Experimental investigation of the peak shear strength criterion based on three-dimensional surface description. Rock Mech Rock Eng 51(4):1005–1025 http://sci-hub.tw/10.1007/s00603-017-1390-0

Lobo-Guerrero S, Vallejo LE (2005) Discrete element method evaluation of granular crushing under direct shear test conditions. J Geotech Geoenviron 131(10):1295–1300. https://doi.org/10.1061/(ASCE)1090-0241(2005)131:10(1295)

Mackenzie FT, Garrels RM (1971) Evolution of sedimentary rocks. Norton, New York

Oh J, Li Y, Mitra R, Canbulat I (2017) A numerical study on dilation of a saw-toothed rock joint under direct shear. Rock Mech Rock Eng 50(4):913–925 http://sci-hub.tw/10.1007/s00603-016-1142-6

Park JW, Song JJ (2009) Numerical simulation of a direct shear test on a rock joint using a bonded-particle model. Int J Rock Mech Min Sci 46(8):1315–1328. https://doi.org/10.1016/j.ijrmms.2009.03.007

Schormair N, Thuro K, Plinninger R (2006) The influence of anisotropy on hard rock drilling and cutting. The Geological Society of London, IAEG, Paper 491: 1–11

Sharma P, Verma AK, Negi A, Jha MK, Gautam P (2018) Stability assessment of jointed rock slope with different crack infillings under various thermomechanical loadings. Arab J Geosci 11(15):431

Sih GC (1974) Strain-energy-density factor applied to mixed mode crack problems. Int J Fract 10(3):305–321. https://doi.org/10.1007/BF00035493

Son BK, Lee YK, Lee CI (2004) Elasto-plastic simulation of a direct shear test on rough rock joints. Int J Rock Mech Min Sci 41:354–359. https://doi.org/10.1016/j.ijrmms.2004.03.066

Song D (2012) Study on evolution process and energy dissipation characteristics of rock burst [D]. China University of Mining and Technology, theses, 2012

Strom A (2006) Morphology and internal structure of rockslides and rock avalanches: grounds and constraints for their modelling. In: Landslides from massive rock slope failure. Springer, Dordrecht, pp 305–326

Sturzenegger M, Stead D (2009) Close-range terrestrial digital photogrammetry and terrestrial laser scanning for discontinuity characterization on rock cuts. Eng Geol 106(3–4):163–182. https://doi.org/10.1016/j.enggeo.2009.03.004

Su SF, Liao HJ, Lin YH (1998) Base stability of deep excavation in anisotropic soft clay. J Geotech Geoenviron 124(9):809–819. https://doi.org/10.1061/(ASCE)1090-0241(1998)124:9(809)

Tang CA, Kaiser PK (1998) Numerical simulation of cumulative damage and seismic energy release during brittle rock failure—part I: fundamentals. Int J Rock Mech Min Sci 35(2):113–121. https://doi.org/10.1016/S0148-9062(97)00009-0

Walsh JJ, Nicol A, Childs C (2002) An alternative model for the growth of faults. J Struct Geol 24(11):1669–1675. https://doi.org/10.1016/S0191-8141(01)00165-1

Wang JA, Park HD (2001) Comprehensive prediction of rockburst based on analysis of strain energy in rocks. Tunn Undergr Space Technol 16(1):49–57. https://doi.org/10.1016/S0886-7798(01)00030-X

Wang SY, Lam KC, Au SK, Tang CA, Zhu WC, Yang TH (2006) Analytical and numerical study on the pillar rockbursts mechanism. Rock Mech Rock Eng 39(5):445–467 http://sci-hub.tw/10.1007/s00603-005-0075-2

Wang SH, Lee CI, Ranjith PG, Tang CA (2009) Modeling the effects of heterogeneity and anisotropy on the excavation damaged/disturbed zone (EDZ). Rock Mech Rock Eng 42(2):229–258 http://sci-hub.tw/10.1007/s00603-009-0177-3

Xiong LX, Chen HJ, Li TB, Zhang Y (2019) Uniaxial compressive study on mechanical properties of rock mass considering joint spacing and connectivity rate. Arab J Geosci 12(21):642

Yan WM (2009) Fabric evolution in a numerical direct shear test. Comput Geotech 36(4):597–603. https://doi.org/10.1016/j.compgeo.2008.09.007

Yan Z, Dai F, Liu Y, Feng P (2019) Experimental and numerical investigation on the mechanical properties and progressive failure mechanism of intermittent multi-jointed rock models under uniaxial compression. Arab J Geosci 12(22):681

Yao J, He F, Xu J (2009) The energy mechanism of rock burst and its application. J Central Soth Univ (NATURAL SCIENCE EDITION) 40(3):808–813 (In Chinese)

Zhang L, Thornton C (2007) A numerical examination of the direct shear test. Geotechnique 57(4):343–354. https://doi.org/10.1680/geot.2007.57.4.343

Zhu WC, Li ZH, Zhu L, Tang CA (2010) Numerical simulation on rockburst of underground opening triggered by dynamic disturbance. Tunn Undergr Space Technol 25(5):587–599. https://doi.org/10.1016/j.tust.2010.04.004